

# Equilibrium Data of Hydrogen, Methane, Nitrogen, Carbon Dioxide, and Natural Gas in Semi-Clathrate Hydrates of Tetrabutyl Ammonium Bromide

Mosayyeb Arjmandi,<sup>†,‡</sup> Antonin Chapoy,<sup>†</sup> and Bahman Tohidi<sup>\*,†</sup>

Centre for Gas Hydrate Research, Institute of Petroleum Engineering, Heriot-Watt University, Edinburgh EH14 4AS, U.K., and Clariant Oil Services, Howe Moss Avenue, Dyce, Aberdeen AB21 0GP, U.K.

Tetrabutyl ammonium bromide (TBAB) forms a semi-clathrate hydrate, which can incorporate small gas molecules such as methane and nitrogen. It has recently been used for separation of gases. However, there are very limited experimental data on the phase boundaries of the gas hydrate form in the presence of TBAB. In this work, we present new experimental data at high-pressure TBAB,  $w = 0.10$ , TBAB ( $w = 0.10$  and  $0.43$ ) + hydrogen, TBAB ( $w = 0.05, 0.10, 0.20$ , and  $0.30$ ) + methane, TBAB ( $w = 0.10$ ) + nitrogen, TBAB ( $w = 0.1$  and  $0.427$ ) + carbon dioxide, and TBAB ( $w = 0.05, 0.10$ , and  $0.43$ ) + natural gas semi-clathrate hydrate phase boundaries. In another part of this work, the results of visual observations of the methane + TBAB semi-clathrate hydrate morphology and the methane gas bubbles released from methane + TBAB semi-clathrate hydrates on dissociation are presented. Finally, the effect of TBAB mass fraction on hydrate promotion and the stability of the new semi-clathrate hydrate are presented.

## Introduction

Gas hydrates are icelike crystalline compounds that are formed by the combination of water molecules and suitably sized “guest” molecules under suitable conditions of pressure and temperature. Water molecules form a lattice structure with cavities that are occupied by gas molecules. The water molecules that form the lattice are strongly hydrogen bonded with each other, and the gas molecule interacts with water molecules through van der Waals type dispersion forces.<sup>1</sup> Tetrabutyl ammonium bromide (hereafter TBAB) in water forms a semi-clathrate hydrate, which shares many of the same physical and structural properties as true clathrate hydrates. The principal difference is that, unlike true clathrates where the guest molecules are not physically bonded within the water structure, in semi-clathrate hydrates, the guest may both form part of the water lattice and occupy cages. The anions are bound to water molecules through hydrogen bonds and form a water + anion framework (host), the cavities of which are occupied by cations (guests).<sup>2</sup> After discovery of the clathrate nature of quaternary ammonium salts,<sup>3</sup> the structures of TBAB semi-clathrate hydrates have been the subject of the investigation of the researchers for many years.<sup>2,4–8</sup> TBAB can form different hydrate structures depending on the equilibrium conditions.<sup>4</sup> The phase diagram and some properties of different TBAB hydrate structures are shown in Figure 1 and Table 1, respectively. As can be seen in Figure 1 and Table 1, different mass fractions of TBAB in water form different hydrate crystals, and as the mass fraction in water increases, the mole ratio of water to TBAB in the crystal structure (hydration number) decreases. The single-crystal morphology of the  $w$  TBAB + H<sub>2</sub>O, with  $w = 0.40$ , semi-clathrate hydrate has been reported to be columnar and to be affected by the degree of subcooling<sup>9</sup> (the temperature

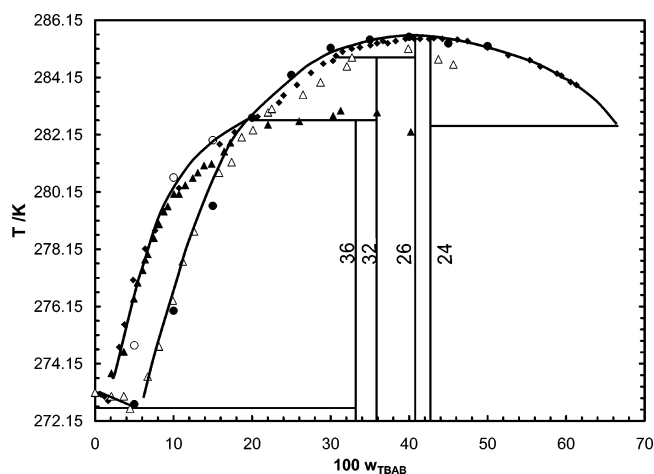


**Figure 1.**  $T, w$  phase diagram of the  $w$  (C<sub>4</sub>H<sub>9</sub>)<sub>4</sub>NBr + H<sub>2</sub>O binary system in the region of crystallization of semi-clathrate polyhydrates.<sup>4</sup> The figures along the lines of compositions are the hydration numbers. ◆, Lipkowski et al.;<sup>6</sup> △, Oyama et al.;<sup>7</sup> ▲, Oyama et al.;<sup>7</sup> ●, Darbouret et al.;<sup>8</sup> ○, Darbouret et al.<sup>8</sup>

difference from equilibrium temperature at equilibrium pressure).

In the recent years, the TBAB semi-clathrate hydrates have been exploited in different technologies by some researchers. TBAB semi-clathrate hydrate has been introduced as a cold storage material because of its higher-phase temperature change compared to that of ice.<sup>10</sup> In addition, the enthalpy of fusion is comparable to that of water, and it forms a slurry that can be transported directly through a pipeline. Shimada and his co-workers<sup>11</sup> used  $w$  TBAB + H<sub>2</sub>O,  $w = 0.10$ , hydrate as a tool for separation of gases. They reported that small molecules such as methane and nitrogen were selectively encaged during  $w$  TBAB + H<sub>2</sub>O,  $w = 0.10$ , hydrate formation, while the larger gas molecules such as ethane and propane were not incorporated into the TBAB hydrate.<sup>12</sup> That was attributed to the small size of TBAB hydrate cages. Later, Shimada and co-workers<sup>20</sup>

\* To whom correspondence should be addressed. E-mail: bahman.tohidi@pet.hw.ac.uk.

<sup>†</sup> Institute of Petroleum Engineering.

<sup>‡</sup> Clariant Oil Services.

**Table 1. Some Known Properties of the Tetrabutyl Ammonium Bromide Semi-Clathrate Hydrate<sup>4a</sup>**

hydrate	$T_F/K$	$\rho/\text{kg}\cdot\text{m}^{-3}$	cell type (space group)	unit cell parameter/ $\text{\AA}$ <sup>o</sup>
$\text{Bu}_4\text{NBr}\cdot 24\text{H}_2\text{O}$	288.55	1123	$C2/m$	$a = 28.5; b = 16.9; c = 16.5; \beta = 125^\circ$
$\text{Bu}_4\text{NBr}\cdot 26\text{H}_2\text{O}$	288.35	1094	$P4/mmm$	$a = 23.9; c = 50.8$
$\text{Bu}_4\text{NBr}\cdot 32\text{H}_2\text{O}$	284.85	1082	$P4/m$	$a = 33.4; c = 12.7$
$\text{Bu}_4\text{NBr}\cdot 36\text{H}_2\text{O}$	282.65	1028	$Pmmm$	$a = 21.3; b = 12.9; c = 12.1$

<sup>a</sup>  $T_F$ , melting point;  $\rho$ , density.

**Table 2. Mole Fraction Composition  $x$  of the Natural Gas (Supplied by BOC Ltd.) Used in This Work**

component	100x
methane	87.32
ethane	5.67
propane	1.68
2-methyl propane	0.23
<i>n</i> -butane	0.40
2-methyl butane	0.10
nitrogen	3.24
carbon dioxide	1.36

reported that in the  $\text{TBAB}\cdot 38\text{H}_2\text{O}$  hydrate crystal two dodecahedral cages could encage small molecules. Therefore, for  $\text{TBAB}\cdot 38\text{H}_2\text{O}\cdot 2\text{CH}_4$  hydrate, the maximum mass fraction of methane is about 3 %.

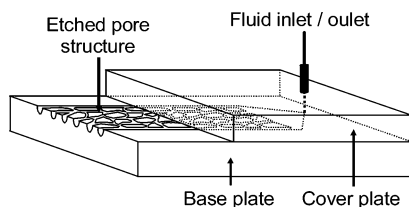
The phase boundaries of double hydrates (when two or more compounds as guests take part in hydrate formation, the resulting hydrate is called double hydrates) of TBAB with different gases will not only be useful in designing gas separation and gas storage and transportation processes but also provide valuable information about different TBAB hydrate structures. Chapoy and co-workers showed that TBAB hydrate could be a potential hydrogen storage media.<sup>13</sup> Tohidi et al. patented the use of quaternary ammonium salts (including TBAB) as a method for gas storage, transport, and other energy applications.<sup>14</sup>

In the first part of this communication, we present the results of the visual observations of TBAB + methane double hydrate dissociation, which denotes incorporation of gas molecules in the TBAB + methane semi-clathrate hydrates. In the second part, the phase boundaries of the TBAB, TBAB + hydrogen, TBAB + methane, TBAB + nitrogen, TBAB + carbon dioxide, and TBAB + natural gas semi-clathrate hydrates are presented.

## Materials and Methods

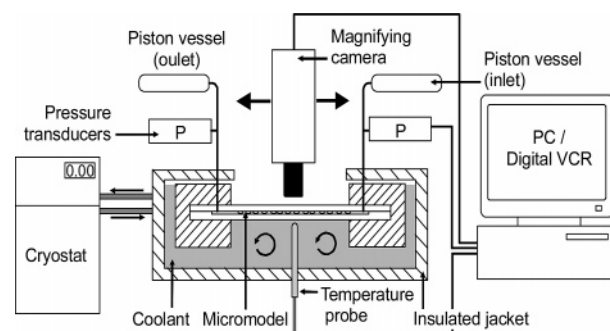
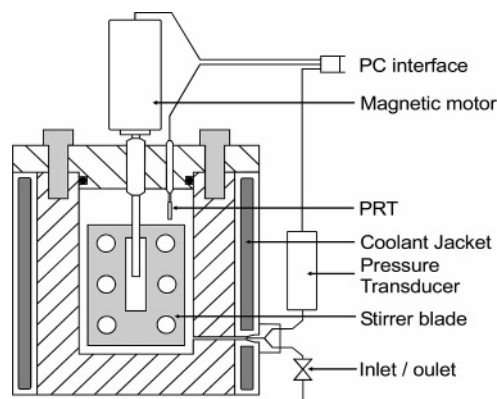
Tetrabutyl ammonium bromide,  $w = 0.50$  in water, was purchased from Aldrich. Deionized water was used to dilute tetrabutyl ammonium bromide to different desired mass fractions in the experiments. Methane (> 99.9 % purity) and carbon dioxide (> 99.9 % purity) were purchased from Air Product Ltd. Hydrogen (> 99.9 % purity), nitrogen (> 99.9 % purity), and natural gas were supplied by BOC Ltd. Table 2 shows the composition of the natural gas used.

The micromodel setup is used to study the morphology of the hydrates. It consists of an etched glass baseplate topped with a sealed glass coverplate (Figure 2). Geometrically designed networks of pores can be used to construct the glass micromodel by etching with hydrofluoric acid. The cover plate has an inlet

**Figure 2.** Cross-section of the glass micromodel.

and outlet, which allows fluids to be pumped through the enclosed network of pores using small-volume piston vessels (Figures 2 and 3). The micromodel is mounted in a vessel, subjected to a confining (overburden) pressure, and fitted into its housing. The setup is submersed in a temperature-controlled bath (GD120 R series, Grant Instruments,  $-25^\circ\text{C}$  to  $100^\circ\text{C}$ ), allowing tests to be carried out under hydrate-forming conditions (Figure 3). Temperature is measured by a probe mounted under the model, and transducers (Druck PDCR960-500 bar pressure transducers) measure pressure on the model inlet and outlet lines. In all experiments, the aqueous (water or TBAB in water solution) phase is dyed with methyl blue to increase the contrast between water, gas bubbles, and hydrates. Gas hydrates exclude methyl blue and appear as white solid particles, while TBAB semi-clathrate hydrate absorbs it and appears as a blue phase. A magnifying camera (JVC, KY-F58) is mounted above the model, and illumination is provided by a cold light source. Because the structure is only one pore thickness deep, it is possible to observe clearly different phases and their changes inside the micromodel. Video footage is recorded during all experiments. The pictures presented here are still images digitally captured from video recordings or directly from the camera.

A Hydrate Kinetic Rig was used in determining hydrate dissociation points (temperature and pressure where the last crystal of hydrates is in equilibrium with water and gas). The

**Figure 3.** Schematic illustration of the micromodel experimental setup.**Figure 4.** Schematic illustration of the Hydrate Kinetic Rig experimental setup.

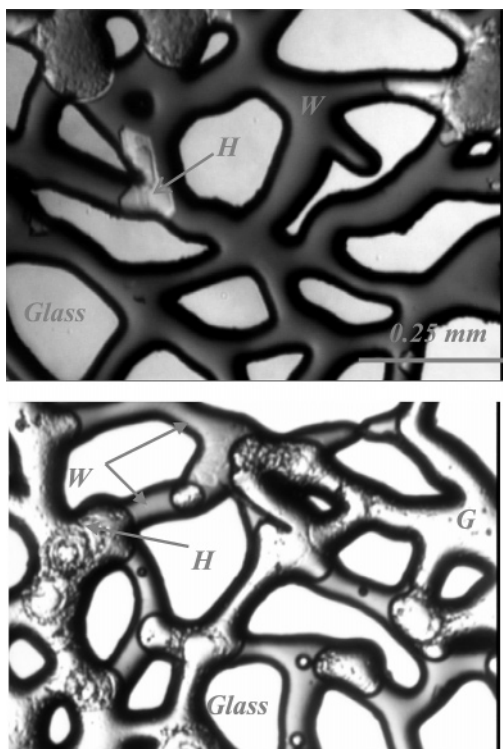
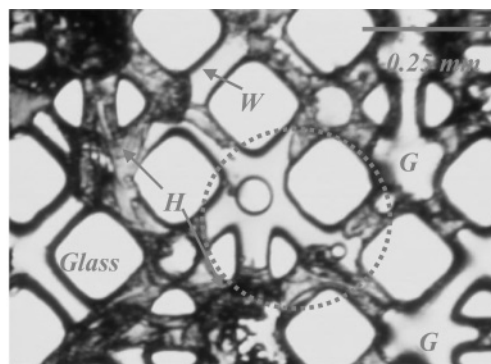


**Figure 5.** Methane hydrate formation and dissociation in water dyed with methyl blue. W, water; H, hydrate; G, gas. First picture: Methane hydrates in water (6.53 MPa, 274.65 K). Second picture: Methane hydrate dissociation in water (6.6 MPa, 282.65 K).

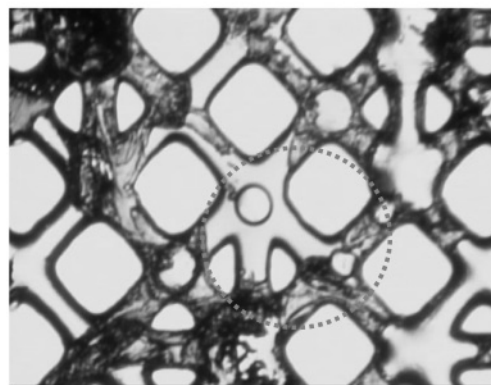
rig, designed and constructed in-house, consists of a 2.4 L high-pressure (40 MPa) vessel (Figure 4). The system temperature was controlled by circulating coolant from a cryostat (GD120 R series, Grant Instruments) within a jacket surrounding the cell. The temperature was measured and monitored by means of a PRT (platinum resistance thermometer) located within the cell ( $\pm 0.2$  K), which was calibrated regularly against a Prema 3040 precision thermometer. The cell pressure was monitored by a Quartzdyne (model QS30K-B, Quartzdyne Inc., U.S.A.) pressure transducer ( $\pm 0.007$  MPa). A stirrer (Top Industrie SA, France, Anchor model 608029800) with a magnetic motor (Top Industrie SA, France, model 6180300B) was used to agitate the test fluids. A computer was used to collect data for pressure and temperature during the experiments. Incipient hydrate–liquid–vapor (H–L–V) and hydrate–liquid (H–L) equilibrium conditions were determined by an isochoric step-heating technique following the method of Tohidi et al.<sup>15</sup>

For hydrate–liquid–vapor (H–L–V) equilibrium, the cell and its loading lines were vacuumed prior to introduction of the TBAB solution, and then the gas was introduced into the cell directly from the commercial cylinder (through preliminary evacuated transfer lines) to a pressure level corresponding to the pressure of the first measurement. More gas was introduced after each measurement up to the highest pressure of the studied system. For hydrate–liquid (H–L) equilibrium, the cell and its loading lines were vacuumed, and then the TBAB was injected using a HPLC (high-pressure liquid chromatography) pump (Hitachi L-6000 Pump) to a pressure level corresponding to the pressure of the first measurement. More solution was introduced after each measurement up to the highest pressure of the studied system.

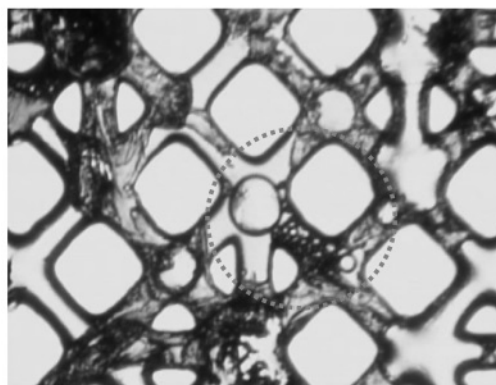
The cell, once charged with test fluids, was first cooled rapidly until clathrate formation was observed (from a pressure reduction associated with gas consumption or from a pressure increase



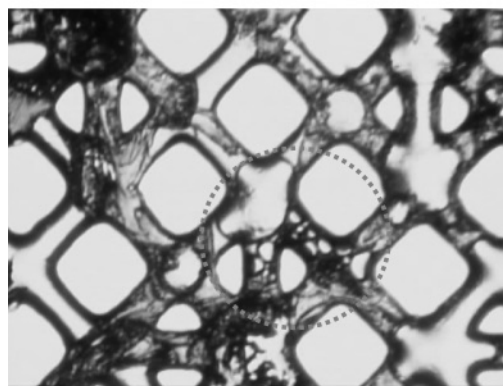
6(a)



6(b)



6(c)



6(d)

**Figure 6.** Sequential still photos of TBAB + methane hydrate dissociation at 8 MPa and 291.85 K. W, water; G, methane gas bubbles; and H, TBAB + methane hydrate dyed with methyl blue coexistence in the micromodel pores is shown. By dissociation, methane gas bubbles are released from the hydrate.

associated with hydrate formation in the case of the pure TBAB hydrate). The temperature was then raised in steps of (3 to 5)



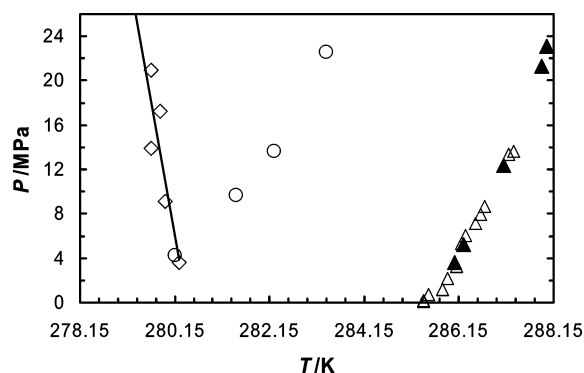


**Figure 7.** TBAB and hydrogen + TBAB hydrate phase boundaries. TBAB system:  $\diamond$ ,  $w = 0.10$  (this work); solid line, best fit to experimental data. Hydrogen + TBAB system:  $\circ$ ,  $w = 0.10$  (this work);  $\blacktriangle$ ,  $w = 0.43$  (this work);  $\triangle$ ,  $w = 0.43$  from Hashimoto et al.<sup>18</sup>

**Table 3.** Measured TBAB,  $w = 0.10$ , Hydrate Dissociation Conditions in the Hydrate–Liquid Region

T/K ( $\pm 0.2$ K)	P/MPa
TBAB, $w = 0.10$	
280.25	3.627
279.95	9.094
279.65	13.893
279.85	17.285
279.65	20.926

K, with sufficient time being given following each temperature step for the system to reach equilibrium (stable pressure), until the point of complete hydrate dissociation was surpassed. Dissociation conditions were then determined isochorically from a heating curve ( $P$ ,  $T$  diagram). The method of step-heating ensures equilibrium at each step, and only equilibrium data were used in determining dissociation conditions. This procedure resulted in reliable and repeatable measurements.<sup>15</sup>

## Results and Discussions

The micromodel setup was used for visual observation of methane hydrate and methane + TBAB,  $w = 0.10$ , double hydrate formation and dissociation. Figure 5 illustrates methane gas hydrate formation and dissociation from methane and water only. As presented in Figure 5(a), methane hydrates formed large white solid plugs in the pores. On dissociation, methane gas releases and coexists with water and methane hydrates (Figure 5(b)). In the presence of TBAB, the morphology of the hydrates formed was different than that of pure methane hydrate. A gel-type hydrate formed which absorbed methyl blue and made the dyed water colorless. Figure 6 shows the sequential still pictures of the methane + TBAB,  $w = 0.10$ , double hydrate dissociation. The release of methane gas bubbles from the hydrate can be observed from the pictures. This denotes the inclusion of methane gas in the TBAB hydrate cages.

The dissociation point data of TBAB double hydrates with different gases were generated in the kinetic rig and compared with the hydrate phase boundaries of the corresponding gases. The TBAB semi-clathrate hydrate phase boundary at atmospheric pressure is shown in Figure 1. The methane, nitrogen, carbon dioxide, and natural gas hydrate phase boundaries were calculated by an in-house model. The details of the model have been explained elsewhere.<sup>16,17</sup> In the first series of experiments, dissociation conditions for TBAB,  $w = 0.10$ , clathrates at elevated pressures were determined (Figure 7) and reported in Table 3. Then, semi-clathrate hydrate phase equilibria were determined experimentally for hydrogen at two different mass fractions of TBAB,  $w = 0.10$  and  $0.43$ , in water under pressures up to 25 MPa (Table 4 and Figure 7).

**Table 4.** Measured Hydrogen + TBAB, ( $w = 0.10$  and  $w = 0.43$ ) Hydrate Dissociation Conditions in the Hydrate–Liquid–Gas Region

T/K ( $\pm 0.2$ K)	P/MPa
TBAB, $w = 0.10$	
280.15	4.233
281.45	9.639
282.25	13.638
283.35	22.532
TBAB, $w = 0.43$	
286.05	3.600
286.25	5.226
287.10	12.411
287.90	21.291
288.00	23.070

**Table 5.** Measured Methane + TBAB,  $w = 0.05, 0.10, 0.20$ , and  $0.30$ , Hydrate Dissociation Conditions in the Hydrate–Liquid–Gas Region

T/K ( $\pm 0.2$ K)	P/MPa
TBAB, $w = 0.05$	
287.15	4.688
288.65	7.040
290.15	10.942
291.65	15.858
292.65	21.160
296.75	41.369
TBAB, $w = 0.10$	
287.15	2.413
289.15	4.482
290.65	6.757
292.65	11.307
294.15	16.306
296.15	24.959
298.15	35.853
TBAB, $w = 0.20$	
287.65	1.421
290.15	3.310
291.65	5.276
293.35	8.028
294.75	12.034
295.65	15.434
TBAB, $w = 0.30$	
291.05	3.283
292.65	5.110
294.25	8.103
295.65	12.124
296.95	17.400

**Table 6.** Measured Nitrogen + TBAB,  $w = 0.10$ , Hydrate Dissociation Conditions in the Hydrate–Liquid–Gas Region

T/K ( $\pm 0.2$ K)	P/MPa
TBAB, $w = 0.10$	
285.15	4.688
288.15	10.945
289.55	16.993
290.15	19.857
291.45	25.683
292.65	31.793
292.95	33.503

In the third series of experiments, the dissociation points of methane–TBAB double hydrate were measured at four different mass fractions of TBAB,  $w = 0.05, 0.10, 0.20$ , and  $0.30$ , in water. The dissociation point data are presented in Table 5. Figure 8 illustrates the dissociation points along with the methane hydrate phase boundary. As presented in Figure 8, the double hydrate formed with TBAB,  $w = 0.05$ , is more stable than methane hydrate at low pressures, and as pressure increases, the temperature difference between methane and the double hydrate dissociation points decreases. At approximately 21.16 MPa, the phase boundaries coincide, and at higher pressures,

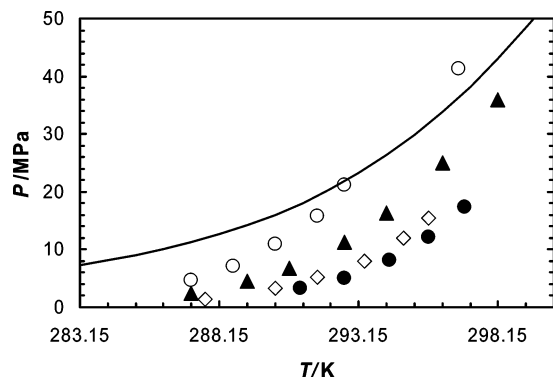


**Figure 8.** Methane + TBAB hydrate phase boundary measured in this work.  $\circ$ ,  $w = 0.05$ ;  $\blacktriangle$ ,  $w = 0.10$ ;  $\diamond$ ,  $w = 0.20$ ;  $\bullet$ ,  $w = 0.30$ ; solid line, methane hydrate phase boundary predicted by an in-house (HWHYD) model.<sup>16,17</sup>

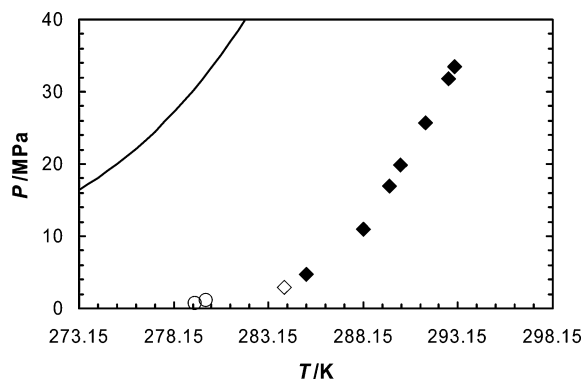


**Figure 9.** Nitrogen + TBAB phase boundary measured in this work.  $\blacklozenge$ , TBAB,  $w = 0.10$ ;  $\circ$ , TBAB,  $w = 0.05$  from Duc et al.;<sup>19</sup>  $\diamond$ , TBAB,  $w = 0.10$  from Duc et al.;<sup>19</sup> solid line, nitrogen hydrate phase boundary predicted by an in-house (HWHYD) model.<sup>16,17</sup>

**Table 7. Measured Carbon Dioxide–TBAB,  $w = 0.10$  and  $0.427$ , Hydrate Dissociation Conditions in the Hydrate–Liquid–Gas Region**

$T/K (\pm 0.2 K)$	$P/MPa$
TBAB, $w = 0.1$	
285.55	1.400
287.35	2.320
289.25	4.090
TBAB, $w = 0.427$	
287.25	1.248
288.75	1.793
290.15	2.896
291.15	3.517

the double hydrate appears to be less stable than methane hydrate. For double hydrates with TBAB,  $w = 0.10$ , the same trend is seen, while in general, it is more stable than the other two hydrates. It should be noted that the dissociation points of TBAB,  $w = 0.05$  ( $x = 0.3\%$ ), and TBAB,  $w = 0.10$  ( $x = 0.6\%$ ), semi-clathrate hydrates are about (277.15 and 279.15) K, respectively (Figure 1).

In the fourth series of experiments, the nitrogen hydrate phase boundaries in the presence of TBAB,  $w = 0.10$ , were measured. The dissociation point data are presented in Table 6. Figure 9 presents the nitrogen hydrate phase boundary along with the nitrogen and TBAB,  $w = 0.10$ , double hydrate phase boundary. As seen, the double hydrate formed is more stable than the nitrogen hydrate, and at lower pressures, the difference between dissociation temperatures of two hydrates increases.

The carbon dioxide hydrate phase boundaries in the presence of TBAB,  $w = 0.10$  and  $0.427$ , were measured in the fifth series

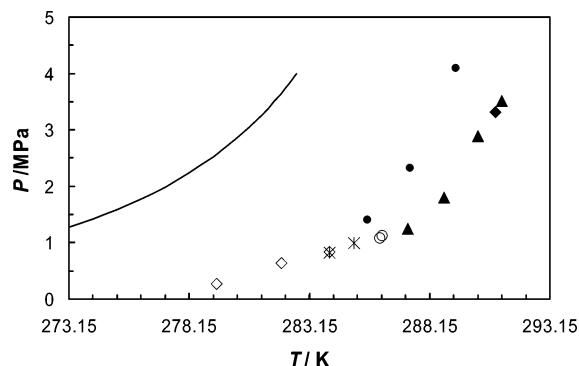


**Figure 10.** Carbon dioxide + TBAB phase boundary measured in this work.  $\bullet$ , TBAB,  $w = 0.10$  (this work);  $\blacktriangle$ , TBAB,  $w = 0.427$  (this work);  $\diamond$ , TBAB,  $w = 0.05$  from Duc et al.;<sup>19</sup>  $\circ$ , TBAB,  $w = 0.10$  from Duc et al.;<sup>19</sup>  $\blacklozenge$ , TBAB,  $w = 0.40$  from Duc et al.;<sup>19</sup>  $*$ , TBAB,  $w = 0.65$  from Duc et al.;<sup>19</sup> solid line, carbon dioxide hydrate phase boundary predicted by an in-house (HWHYD) model.<sup>16,17</sup>

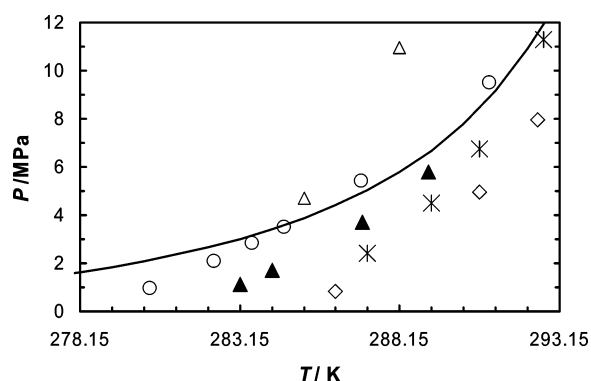


**Figure 11.** Natural gas + TBAB phase boundary measured in this work. Natural gas composition is shown in Table 2. Natural gas system:  $\circ$ , TBAB,  $w = 0.05$ ;  $\blacktriangle$ , TBAB,  $w = 0.10$ ;  $\diamond$ , TBAB,  $w = 0.43$ ; solid line, natural gas hydrate phase boundary predicted by an in-house (HWHYD) model.<sup>16,17</sup> Methane system:  $*$ , TBAB,  $w = 0.10$ . Nitrogen system:  $\triangle$ , TBAB,  $w = 0.10$ .

**Table 8. Measured Natural Gas + TBAB,  $w = 0.05$ ,  $0.10$ , and  $0.43$ , Hydrate Dissociation Conditions in the Hydrate–Liquid–Gas Region**

$T/K (\pm 0.2 K)$	$P/MPa$
TBAB, $w = 0.05$	
280.35	0.979
282.35	2.068
283.55	2.854
284.55	3.482
286.95	5.419
290.95	9.515
TBAB, $w = 0.10$	
283.15	1.145
284.15	1.720
286.97	3.694
289.05	5.812
TBAB, $w = 0.43$	
286.15	0.828
290.65	4.972
292.45	7.966

of experiments. The dissociation point data are presented in Table 7. Figure 10 presents the carbon dioxide hydrate phase boundary along with carbon dioxide and TBAB,  $w = 0.10$  and  $0.427$ , double hydrate phase boundaries. As presented in Figure 10, the double hydrate formed is more stable than the carbon dioxide hydrate.

The hydrate phase boundaries and measured dissociation points of natural gas (the composition is shown in Table 2) with TBAB,  $w = 0.05$ ,  $0.10$ , and  $0.43$ , are presented in Figure 11

and Table 8. For comparison, methane + TBAB,  $w = 0.10$ , and nitrogen + TBAB,  $w = 0.10$ , are also shown in Figure 11. In the range of pressures shown in Figure 11, methane + TBAB,  $w = 0.10$ , hydrates are more stable than natural gas + TBAB,  $w = 0.10$ , hydrates. The phase boundary of the natural gas + TBAB,  $w = 10$ , hydrate lies between methane + TBAB and nitrogen + TBAB.

## Conclusions

In this work, the morphology of tetrabutyl ammonium bromide + methane double hydrate was studied, and it was shown that methane gas molecules are included in the TBAB semi-clathrate hydrate. The phase boundaries of TBAB and different gases double hydrates were measured. The results showed that, in general, semi-clathrates of TBAB and gases studied in this work are more stable than common hydrates at low-pressure conditions, but this may change at high-pressure conditions, in particular for semi-clathrates formed with low concentrations of TBAB. The effect of TBAB concentration on the stability of the double hydrates was studied, and it was shown that hydrate stability increases with TBAB concentration.

## Literature Cited

- (1) Sloan, E. D. *Clathrate Hydrates of Natural Gases*, 2nd ed.; Marcel Dekker: New York, 1998.
- (2) Jeffrey, G. A.; McMullan, R. K. *Progress in Inorganic Chemistry*; John Wiley: New York, 1967; Vol. 8, pp 43–108.
- (3) Fowler, D. L.; Loebenstein, W. V.; Pall, D. B.; Kraus, C. A. Some unusual hydrates of quaternary ammonium salts. *J. Am. Chem. Soc.* **1940**, *62*, 1140–1142.
- (4) Dyadin, Y. A.; Udachin, K. A. Clathrate formation in water-peralkylonium salts systems. *J. Inclusion Phenom.* **1984**, *2*, 61–72.
- (5) Davidson, D. W. *Water—A comprehensive treatise*; Plenum Press: New York, 1973.
- (6) Lipkowski, J.; Komarov, V. Y.; Rodionova, T. V.; Dyadin, Y. A.; Aladko, L. S. The structure of Tetra-butyl-ammonium bromide hydrate ( $C_4H_9$ )<sub>4</sub>NBr·2 1/3 H<sub>2</sub>O. *J. Supramol. Chem.* **2002**, *2*, 435–439.
- (7) Oyama, H.; Shimada, W.; Ebinuma, T.; Kamata, Y.; Takeya, S.; Uchida, T.; Nagao, J.; Narita, H. Phase diagram, latent heat, and specific heat of TBAB semiclathrate hydrate crystals. *Fluid Phase Equilib.* **2005**, *234*, 131–135.
- (8) Darbouret, M.; Courmil, M.; Herri, J.-M. *Rheological study of a hydrate slurry for air conditioning application*, Proceedings of the fifth international conference on gas hydrates, Trondheim, Norway, June 12–16, 2005.
- (9) Shimada, W.; Ebinuma, T.; Oyama, H. Y.; Takeya, S.; Uchida, T.; Nagao, J.; Narita, H. *Growth mechanism of semi-clathrate hydrate single crystals*, Proceedings of the fourth international conference on gas hydrates. Yokohama, May 19–23, 2002; pp 557–560.
- (10) Tanasawa, I.; Takao, S. *Clathrate hydrate slurry of tetra-butyl ammonium bromide as a cold storage material*, Proceedings of the fourth international conference on gas hydrates. Yokohama, May 19–23, 2002; pp 963–967.
- (11) Shimada, W.; Ebinuma, T.; Oyama, H.; Kamata, Y.; Takeya, S.; Uchida, T.; Nagao, J.; Narita, H. Separation of gas molecule using tetra-n-butyl ammonium bromide semi-clathrate hydrate crystals. *Jpn. J. Appl. Phys.* **2003**, *42*, 129–131.
- (12) Kamata, Y.; Oyama, H.; Shimada, W.; Ebinuma, Y.; Takeya, S.; Uchida, T.; Nagao, J.; Narita, H. Gas separation method using tetra-n-butyl ammonium bromide semi-clathrate hydrate. *Jpn. J. Appl. Phys.* **2004**, *43*, 362–365.
- (13) Chapoy, A.; Anderson, R.; Tohidi, B. Low pressure molecular hydrogen storage in semi-clathrate hydrates of quaternary ammonium compounds. *J. Am. Chem. Soc.* **2007**, *129*, 746–747.
- (14) Tohidi, B.; Yang, J.; Chapoy, A.; Arjmandi, M.; Anderson, R. A method for gas storage a, transport and energy generation. Int. Patent., 2006, WO2006/131738.
- (15) Tohidi, B.; Burgass, R. W.; Danesh, A.; Østergaard, K. K.; Todd, A. C. Improving the accuracy of gas hydrate dissociation point measurements. *Ann. N.Y. Acad. Sci.* **2000**, *912*, 924–931.
- (16) Tohidi-Kalorazi, B. Gas hydrate equilibria in the presence of electrolyte solutions. Ph.D. Thesis, Heriot-Watt University, 1995.
- (17) Tohidi, B.; Danesh, A.; Todd, A. C. Modeling single and mixed electrolyte solutions and its applications to gas hydrates. *Chem. Eng. Res. Des.* **1995**, *73A*, 464–472.
- (18) Hashimoto, S.; Murayama, S.; Sugahara, T.; Sato, H.; Ohgaki, K. Thermodynamic and Raman spectroscopic studies on H<sub>2</sub> + tetrahydrofuran + water and H<sub>2</sub> + tetra-n-butyl ammonium bromide + water mixtures containing gas hydrates. *Chem. Eng. Sci.* **2006**, *61*, 7884–7888.
- (19) Duc, N. H.; Chauvy, F.; Herri, J.-M. CO<sub>2</sub> capture by hydrate crystallization – A potential solution for gas emission of steelmaking industry. *Energy Convers. Manage.* **2007**, *48*, 1313–1322.
- (20) Shimada, W.; Shiro, M.; Kondo, H.; Takeya, S.; Oyama, H.; Ebinuma, T.; Narita, H. Tetra-n-butyl ammonium bromide – water (1/38). *Acta Crystallogr.* **2005**, *C61*, 065–066.

Received for review March 23, 2007. Accepted September 14, 2007. This work is part of a project supported by the UK Engineering and Physical Science Research Council (EPSRC Grant GR/N06724/01), which is gratefully acknowledged.

JE700144P